Journal of Polymers and the Environment (2025) 33:5163–5179
https://doi.org/10.1007/s10924-025-03692-4

ORIGINAL PAPER

Synthesis of Block Copolymers Through Melt Polymerization for Compatibilizing PLA/PBAT Blends

Mi Kyung Kwon[1] · Young Jae Lee[1] · Se Geun Lee[1] · Sang Gu Kim[2] · Sung Jun Lee[1]

Received: 6 July 2025 / Accepted: 20 September 2025 / Published online: 4 November 2025

Abstract
Block copolymers, unlike reactive compatibilizers, can stably localize at the interface without reducing biodegradation rate, making them attractive compatibilizers for PLA/PBAT blends. For industrial use, they should be synthesized from commercial PBAT by melt polymerization to lower costs. However, melt polymerization is exposed to ambient moisture, leading to concurrent formation of PLA homopolymer. In this study, PLA–PBAT block copolymers were synthesized by both solution and melt polymerization with different lactide feed ratios. Melt polymerization was performed in an internal mixer as a precursor to reactive extrusion. Products were characterized by NMR, FT-IR, GPC, DSC, and TGA, and performance in blends was evaluated using DSC, SEM, and UTM. Melt samples displayed two cold crystallization peaks. The high-temperature peak corresponded to PLA homopolymer and became more pronounced with increasing lactide feed ratio. This suggests that excess lactide was consumed in homopolymerization. The presence of PLA homopolymer was more clearly observed in DTA than in GPC. In blends, melt samples improved tensile strength gradually with increasing lactide ratio, whereas solution samples showed the highest strength at a 1:1 PBAT-to-lactide ratio. At the ratio, the blend with solution samples exhibited higher tensile strength than that with melt samples. However, this difference was mitigated when melt samples with higher lactide ratios were incorporated at contents of 5 phr or less. The pristine blend formed metastable α′ crystals, while melt-sample-containing blends exhibited both α and α′ structures, with the α form becoming more dominant at higher lactide ratios.

Keywords PLA/PBAT blend · PLA-PBAT block copolymer · Melt polymerization · PLA homopolymer · Differential thermal analysis (DTA)

Introduction

Polylactic acid (PLA) is an aliphatic polyester derived from renewable resources and is known to be fully biodegradable under industrial composting conditions. Above all, PLA exhibits a high elastic modulus and tensile strength comparable to conventional petroleum-based plastics, making it one of the most promising alternatives to non-degradable polymers. However, PLA suffers from inherent drawbacks such as low flexibility, high brittleness, slow crystallization rate, and low melt strength. To overcome these limitations, PLA-based biodegradable materials are typically developed through blending with other biodegradable polymers that possess complementary properties, such as poly(butylene adipate-*co*-terephthalate) (PBAT), thermoplastic starch (TPS), and poly(butylene succinate) (PBS). Among them, the PLA/PBAT blend was first proposed by Jiang et al. [1] in 2005. Owing to its high elongation at break and excellent flexibility, PBAT has been shown to enhance the elongation at break of PLA from 3.8% to over 200% with only a 5 wt% addition. However, due to the intrinsic structural differences between PLA and PBAT, such as chain rigidity, crystallinity, and weak interfacial adhesion, the two polymers exhibit poor compatibility. When more than 5 wt% of PBAT is added, phase separation occurs, leading to a deterioration in tensile strength [2]. To develop highly ductile products such as biodegradable melt-blown films, it is necessary to

✉ Sung Jun Lee
schrisj@dgist.ac.kr

[1] Division of Biomedical Technology, Daegu Gyeongbuk Institute of Science & Technology (DGIST), Daegu, Republic of Korea

[2] R&D Center, Woosung Chemical Co., Ltd, Yeongcheon, Republic of Korea

increase the PBAT content in the blend significantly. To prevent phase separation even at high PBAT content, it is essential to introduce a compatibilizer that enhances the interfacial adhesion between PLA and PBAT.

Numerous researchers have developed numerous compatibilization strategies, broadly categorizing them into reactive and non-reactive categories [3, 4]. The reactive compatibilization involves inducing chemical reactions during the blending of PLA and PBAT [5]. In compounding, in-situ grafting reactions between PLA and PBAT can be promoted by introducing multifunctional additives such as glycidyl methacrylate (GMA) [6, 7], Joncryl ADR [8–12], and methylene diphenyl diisocyanate (MDI) [13], by adding a radical initiator such as dicumyl peroxide (DCP) [14–16], by adding a transesterification catalyst [17, 18], or by replacing either PLA or PBAT with their maleic anhydride-grafted forms [19]. The challenge lies in the fact that these reactions don't solely take place at the interface. Reactive additives can also act as chain extenders, which are known to significantly reduce the degradation rate of biodegradable materials [20]. Researchers have extensively studied the compatibilization approach using reactive additives over the years, but efforts to overcome these limitations are still ongoing [21].

Non-reactive compatibilization includes methods such as Pickering-like compatibilization, electrostatic interaction-based compatibilization, and compatibilization via the incorporation of block copolymers. Pickering-like compatibilization refers to the strategy in which solid nanoparticles selectively localize at the interface of immiscible blends, forming a physical barrier and reducing interfacial tension. The incorporated nanoparticles induce interfacial jamming, thereby suppressing droplet coalescence and stabilizing a co-continuous structure [22, 23]. However, this approach has several limitations. First, it is difficult to precisely control the dispersion and interfacial localization of nanoparticles, and aggregation may even induce interfacial defects [24, 25]. In addition, the use of inorganic nanoparticles can reduce transparency and increase viscosity, thereby impairing processability. Electrostatic interaction-based compatibilization enhances interfacial adhesion by inducing Coulombic attraction or ionic bonding at the interface. Additives such as ionomers [26, 27] and ionic liquids [28, 29] are typically employed. This strategy allows the fine-tuning of interfacial properties by adjusting ionic functional groups, pH, and charge density. In contrast, its drawback is that electrostatic forces are easily screened by humidity, moisture, or salt concentration, which makes the system highly sensitive to environmental conditions [30, 31].

Block copolymers align at the interface between the two phases, thereby reducing the interfacial energy and minimizing the overall free energy of the blend. Interfacial adhesion is achieved through the formation of entanglements (i.e., physical bonding) between each segment of the block copolymer and either PLA or PBAT. Furthermore, semi-crystalline polymers can further stabilize the interface by forming co-crystallization when the segments of the block copolymer are sufficiently long [4]. For a block copolymer to act effectively as a compatibilizer, an appropriate amount must be incorporated. Within the blend, it should rapidly diffuse to the interface and form entanglements (or co-crystallization) with the blend components, thereby achieving stable localization at the interface. Sun et al. [32] reported that the incorporation of two triblock copolymers with different molar masses into a PLA/PBAT blend exhibited a synergistic effect on compatibility. Short-segment block copolymers primarily improved the mobility of the compatibilizer, whereas long-segment block copolymers contributed to interfacial adhesion. Their simultaneous incorporation resulted in complementary actions.

Block copolymers, one of the oldest subjects in polymer science, are regarded as a well-established compatibilization strategy. This is due to the progressive development of theoretical studies based on interfacial physics and modelling [33, 34], along with the extensive accumulation of experimental results across various blend systems [35]. In recent years, growing interest in sustainability has brought renewed attention to block copolymers in the context of mechanical recycling of plastics [4, 36]. When mixed waste streams are mechanically recycled, severe phase separation between incompatible components often leads to significant deterioration in performance. The renewed interest in block copolymers stems from efforts to enhance the competitiveness of recycled blends through the use of well-designed compatibilizers. In particular, recent studies based on molecular dynamics simulations have enabled more efficient structural design of block copolymers as compatibilizers [37].

Although block copolymers have long been recognized for their ability to improve interfacial adhesion, their industrial application has been limited by the high production costs associated with conventional solution or suspension polymerization methods. In 1996, Stevels et al. [38] proposed a cost-effective method for synthesizing block copolymers by co-extruding poly(ε-caprolactone) and lactide via reactive extrusion in the presence of stannous octoate, achieving high yield. Since then, the synthesis of block copolymers via reactive extrusion has been further explored by various researchers [39, 40], but widespread industrial adoption has been limited due to technical challenges in the reactive extrusion and strong demand for low-cost alternative compatibilizers, such as reactive additives. However, the recent resurgence of interest in block copolymers is supported by the growing demand for well-defined compatibilizers and

the accumulation of technological advancements in reactive extrusion. As a result, reactive extrusion is once again gaining attention as a scalable, solvent-free platform for the production of functional block copolymers [41, 42].

Sun et al. [32] and Ding et al. [43] synthesized PLA–PBAT–PLA triblock copolymers and demonstrated their effectiveness in enhancing the compatibility of PLA/PBAT blends. In their studies, solution polymerization was employed for the ring-opening polymerization of lactide, with PBAT synthesized separately and used as a macro-initiator. Notably, the macro-initiators they used had a lower molar mass than the commercial PBAT employed in the present study. For PLA–PBAT block copolymers to be viable as industrial compatibilizers, however, it is essential to replace the conventional solution polymerization method with reactive extrusion and to utilize commercially available PBAT as a macro-initiator. This strategy would enhance cost competitiveness, making PLA–PBAT copolymers more comparable to other commercial compatibilizers. In this study, PLA–PBAT block copolymers were synthesized using commercial PBAT as a macro-initiator. Two different routes of copolymerization were explored: solution polymerization as a conventional production method and melt polymerization as a precursor to reactive extrusion. We synthesized PLA–PBAT block copolymers via two polymerization routes and compared not only their intrinsic properties but also their performance when incorporated into PLA/PBAT blends.

Experimental

Materials

$_{L}$-lactide (Product No. 367044), stannous octoate(tin(II) 2-ethylhexanoate, Product No. 287172), and anhydrous toluene (Product No. 244511) were all purchased from Sigma-Aldrich. $_{L}$-lactide was simply referred to as lactide. Chloroform and ethyl alcohol, which were used as solvents in the precipitation process, were obtained from Honeywell (HPLC grade) and Samchun Pure Chemical (purity 94.5%), respectively. The polymer resins PLA and PBAT were purchased from NatureWorks (Grade: 2003D) and Lotte Fine Chemical (Grade: EnPol PBG7070), respectively.

Table 1 The actual weights of materials used in the Preparation of each sample

Sample name	PBAT [g]	Lactide [g]	Catalyst	$m_{Lactide}/m_{PBAT}$
S0.3	27 g	9 g	0.5wt% of Lactide	≈0.3
S1	18 g	18 g		1
S2	12 g	24 g		2
S3	9 g	27 g		3

Copolymerization Via Solution Polymerization

Block copolymers were synthesized via the ring-opening polymerization of lactide in anhydrous toluene, using commercial PBAT with hydroxyl end groups as a macro-initiator and stannous octoate as a catalyst. The solution polymerization method was adapted from Ding et al. [43]. Prior to use, PBAT and lactide were vacuum-dried at 80 °C and 50 °C, respectively, for 12 h. PBAT and lactide were used in total amounts of 36 g with weight ratios of 3:1, 1:1, 1:2, and 1:3. And the catalyst was added at 0.5 wt% relative to lactide. The reactants and catalyst were placed in a 250 mL three-neck flask, which was then purged with nitrogen. As a reaction solvent, 40mL of anhydrous toluene was added via syringe. Ring-opening polymerization was carried out under a nitrogen atmosphere at 120 °C for 24 h. The resulting product was dissolved in chloroform and precipitated three times in chilled ethyl alcohol. The precipitate was collected by filtration and vacuum-dried at 50 °C for 12 h. These samples of block copolymers were labeled S0.3, S1, S2, and S3, according to the feed ratio of lactide relative to PBAT, as summarized in Table 1.

Copolymerization Via Melt Polymerization

Here, PBAT (macro-initiator), lactide (monomer), and stannous octoate (catalyst) were mixed in an internal mixer (Brabender Plasti-Corder Lab-Station) to synthesize a block copolymer without a solvent. This solvent-free ring-opening polymerization in the PBAT melt was termed melt polymerization. This term implies that the ultimate goal of this study is to manufacture a block copolymer through reactive extrusion. PBAT and lactide were blended in various weight ratios (3:1, 3:2, 1:1, and 2:3) with a total mass of 45 g. Both PBAT and lactide were vacuum-dried prior to use. The amount of catalyst was set to 0.5 wt% relative to lactide. Due to the higher polymerization temperature compared to the solution method, two antioxidants—Irganox 1010 and Irgafos 168—were added at 0.1 phr each. All components (PBAT, lactide, catalyst, and antioxidants) were premixed prior to polymerization. The mixture was charged into the internal mixer, and melt polymerization was carried out at 170 °C with a screw speed of 50 rpm. The reaction time was set to 40 min, corresponding to the torque plateau.

In contrast to the three-neck flask used in solution polymerization, the chamber of the internal mixer consists of three metallic heating blocks, which may allow molten lactide to escape. Moreover, while the vertically oriented stirrer in the solution system facilitates efficient mixing, the screws in the internal mixer are aligned horizontally. As a result, the

Table 2 The actual weights of materials used in the Preparation of each sample

Sample name	PBAT [g]	Lactide [g]	Catalyst	$m_{Lactide}/m_{PBAT}$
M0.3	33.75 g	11.25 g	0.5wt% of Lactide	≈0.3
M0.6	27 g	18 g		≈0.6
M1	22.5 g	22.5 g		1
M1.5	18 g	27 g		1.5

mixing efficiency in the melt system was strongly affected by the viscosity of the reactants. Therefore, the maximum feed ratio of lactide to PBAT was limited to 1.5:1 in melt polymerization. These products were designated as M0.3, M0.6, M1, and M1.5, based on the feed ratio of lactide to PBAT, as summarized in Table 2.

Compatibilization of PLA/PBAT Blend

The same PBAT as the macro-initiator was used as a blend component. The composition of the blend was fixed at a weight ratio of 45:55 (PLA: PBAT). All pellets were vacuum-dried at 80 °C for 12 h prior to use. The compatibilizers synthesized above were incorporated at concentrations of up to 10 wt%, along with 0.1 phr each of Irganox 1010 and Irgafos 168 as antioxidants. Blending was performed using the same internal mixer employed for melt polymerization, operated at 185 °C and 50 rpm for 10 min.

Characterization

^{1}H-Nuclear magnetic resonance (^{1}H-NMR) spectra were acquired using a Bruker AVANCE III spectrometer with deuterated chloroform ($CDCl_3$) as the solvent at ambient temperature. Fourier-transform infrared (FT-IR) spectroscopy was conducted using a Thermo Scientific Nicolet Continuum equipped with an attenuated total reflectance (ATR) module. Spectra were recorded at ambient temperature in the range of 800–4000 cm^{-1} with a resolution of 0.09 cm^{-1}. Gel permeation chromatography (GPC) measurements were conducted on a Waters Alliance e2695 system equipped with a refractive index (RI) detector. The system employed Styragel HR3, HR4, and HR5E columns. Chloroform served as the mobile phase, delivered at 1.0 mL/min, with the column oven maintained at 35 °C. Differential scanning calorimetry (DSC) analysis was performed using a TA Instruments Discovery DSC. Each sample was sealed in a hermetic aluminum pan and subjected to the following thermal protocol: heating from room temperature to 200 °C at a rate of 10 °C/min, holding for 10 min, cooling to −40 °C at 10 °C/min, and reheating to 200 °C at the same rate. Thermogravimetric analysis (TGA) was carried out with a TA Instruments Auto Q500. Specimens were heated from 25 °C to 700 °C at 20 °C/min under a nitrogen purge (60 mL/min). The thermal decomposition temperature was defined by the maximum in the differential thermal analysis (DTA) curve, and the local minima in DTA were used to distinguish each decomposition stage. Tensile properties were examined using a universal testing machine (UTM, United Calibration SFM-100kN) following the ASTM D638 protocol. Dumbbell-shaped specimens with a length of 20 mm, width of 4 mm, and thickness of 1 mm were tested at a crosshead speed of 100 mm/min. We repeated seven times, and after excluding the maximum and minimum values, the mean and standard deviation were calculated from the remaining five data points. The microstructure morphology of blends was observed by scanning electron microscopy (SEM, Hitachi SU8020). Prior to imaging, samples were fractured in liquid nitrogen and sputter-coated with platinum for 60 s. The accelerating voltage was set to 3.0 kV.

Table 3 Molar mass characteristics of polymer resins, as determined by GPC

Type	Grade	M_n [g/mol]	M_w [g/mol]	Dispersity	Supplier
PBAT	PBG7070	52,100	138,000	2.65	Lotte Fine Chemical
PLA	2003D	182,100	380,400	2.09	NatureWorks

Results and Discussion

Characterization of PBAT as a macro-initiator

Table 3 summarizes the molar mass characteristics of the polymer resins measured by GPC. The acid number (n) of PBG7070 used as a macro-initiator is known to be approximately 1.2 mg KOH/g. According to Eq. (1), the concentration of carboxyl groups (c) is calculated to be 21.4 µmol/g.

$$c\ [\mathrm{mol\,COOH/g\,PBAT}] = \frac{n\ [\mathrm{mg\,KOH/g\,PBAT}]}{56.1 \times 10^3\ [\mathrm{mg\,KOH/mol\,KOH}]} \quad (1)$$

$$c'\ [\mathrm{mol\ COOH/mol\,PBAT}] = M_n\ [\mathrm{g\,PBAT/mol\,PBAT}] \times c\ [\mathrm{mol\,COOH/g\,PBAT}] \quad (2)$$

When the number-average molar mass from Table 3 is applied, this corresponds to 1.1 mol of carboxyl end groups per mole of PBG7070. Therefore, when PBG7070 is used as a macro-initiator, the resulting block copolymer is expected to have a di-block structure.

Characterization of Block Copolymer Via Different Polymerization

Figure 1 shows the ^{1}H-NMR spectra of PBAT as the macro-initiator and S1 as a block copolymer. PBAT is a random copolymer composed of a butanediol–adipate (BA) unit and a butanediol–terephthalate (BT) unit. The BT repeating unit is characterized by aromatic protons of the benzene ring at 8.11 ppm (*a*) and by the methylene protons of butanediol, appearing at 4.38–4.46 ppm (outer -CH_2-, *b*) and 1.66 ppm (inner -CH_2-, *e*) [43]. The methylene protons in the BA repeating unit appear at 2.34ppm (outer -CH_2- in adipic acid, *d*), 1.67-1.67.67.67.69ppm (inner -CH_2- in adipic acid, *g*), 4.11-4.11.11.11.17ppm (outer -CH_2- in butanediol, *c*), and 1.69ppm (inner -CH_2- in butanediol, *h*) [43]. The two triplet peaks around 3.7ppm are assigned to the methylene protons (*i*) in the butanediol adjacent to the hydroxyl end group [43].

For PBAT, the integral areas of peaks *a* (representing the BT unit) and *d* (representing the BA unit), relative to the end-group peak (*i*), were determined to be 59.6 and 62.2, respectively. Based on the NMR results and the acid value of PBAT, the molar mass was calculated to be approximately 12,800 g/mol, which is about one-quarter of the

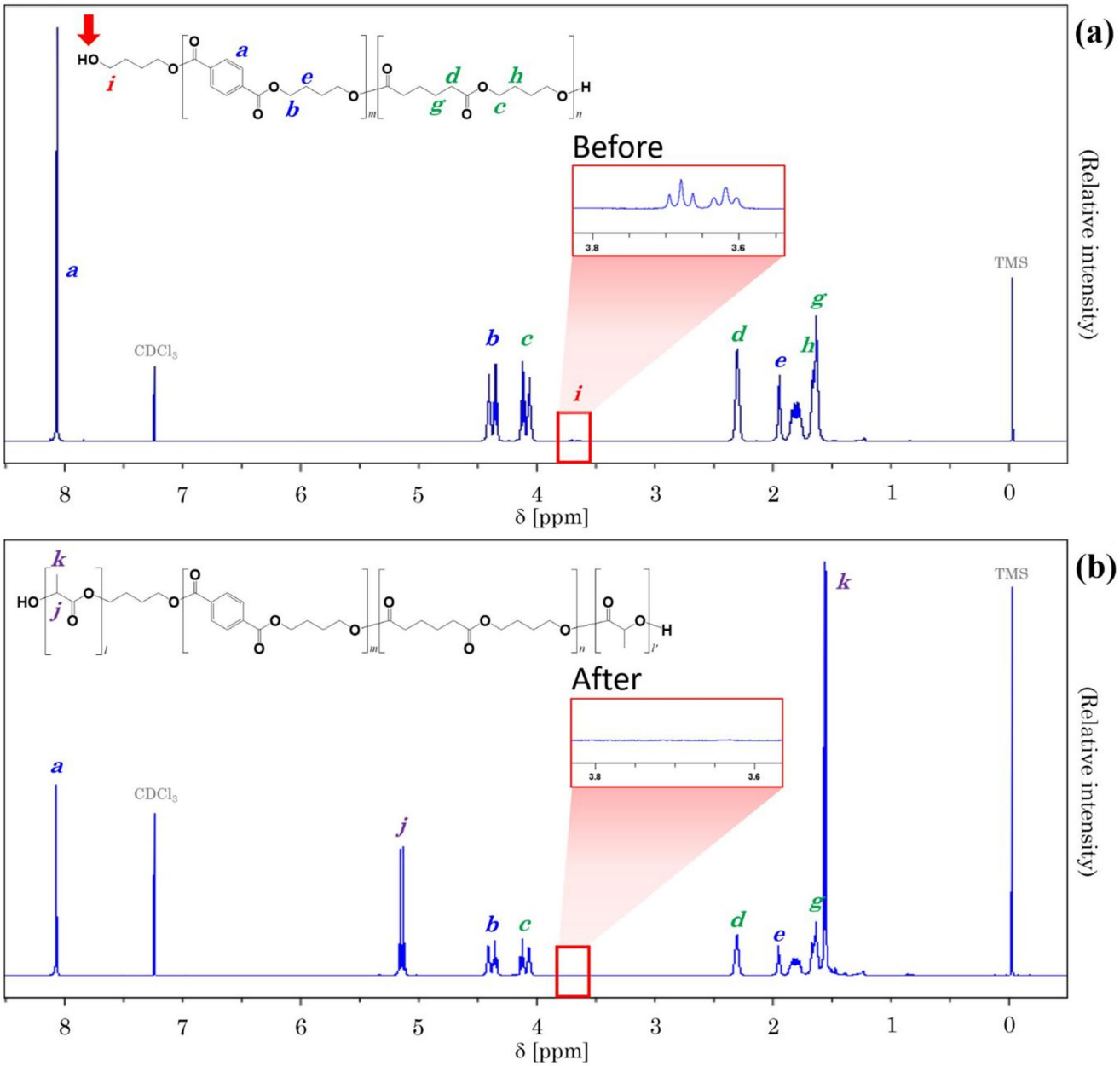

Fig. 1 ^{1}H-NMR spectra of (a) PBAT as the macro-initiator and (b) S1 as a block copolymer: Disappearance of the methylene peak adjacent to the hydroxyl end group after polymerization

number-average molar mass obtained from GPC. Although the molar mass derived from NMR corresponds to the absolute value, its accuracy decreases for high-molar-mass polymers because the end-group signals become too weak to be quantified reliably [44].

When lactide is polymerized from the hydroxyl end group of PBAT, these triplet signals representing the hydroxyl end group (*i*) disappear. All synthesized products exhibited this disappearance, confirming successful initiation of lactide polymerization at the PBAT hydroxyl end group. The PLA-PBAT block copolymer consists of three repeating units: the BT and BA units from the PBAT segment and the lactide unit from the PLA segment. Upon the polymerization of lactide, characteristic signals of PLA segments emerge at 5.09 ppm (main-chain methine proton, *j*) and 1.49 ppm (methyl protons, *k*) [43]. Table 4 presents the ratios of repeating units in the solution and melt samples, obtained from the integral values of the characteristic peaks corresponding to each repeating unit (*a* for the BT unit, *d* for the BA unit, and *j* for the lactide unit).

In the case of solution samples, polymerization proceeds in a nitrogen-purged reactor, allowing the ratio of lactide units in Table 4 to be regarded as proportional to the degree of polymerization (DP) of the PLA segment in the block copolymer. In contrast, the melt samples are polymerized under atmospheric conditions, where exposure to moisture may initiate the formation of PLA homopolymer (or oligomer), which is likely to coexist with the block copolymer. Therefore, for the melt samples, the ratio of lactide units in Table 4 cannot be directly interpreted as the DP of the PLA segment in the block copolymer. In both the solution and melt samples, the ratio of the lactide units observed in the ^{1}H-NMR spectra increases with the lactide feed ratio. When comparing samples with the same lactide feed ratio, S1 and M1 exhibited similar lactide unit ratios of 4.48 and 4.89, respectively. However, a pronounced discrepancy was observed between S0.3 and M0.3, with lactide unit ratios of 0.35 and 1.82, respectively—indicating that M0.3 contained more than five times the lactide content of S0.3.

Hereafter, the copolymers synthesized by solution polymerization are referred to as solution samples, whereas the products obtained via melt polymerization are referred to as melt samples. This distinction is made because the products of solution polymerization are primarily composed of well-defined block copolymers, whereas those obtained from melt polymerization are expected to contain a mixture of block copolymers and PLA homopolymers.

Table 4 The ratios of repeating units in each sample determined by ^{1}H-NMR spectra

PBAT segment		Solution sample	Lactide unit	Melt sample	Lactide unit
BT unit	BA unit				
1	1.04	S0.3	0.35	M0.3	1.82
		S1	4.48	M0.6	3.64
		S2	10.78	M1	4.89
		S3	15.92	M1.5	6.67

Figure 2 presents the FT-IR spectra of the solution and melt samples. The bands at 2958 cm^{-1} and 1714 cm^{-1} are characteristic of PBAT, corresponding to the asymmetric stretching vibration of CH_2 and the stretching vibration of C=O, respectively. After the ring-opening polymerization of lactide, new bands appeared at 2995 cm^{-1}, 1746 cm^{-1}, 1361 cm^{-1}, and 1182 cm^{-1}, which are characteristic of PLA. These bands are attributed to the asymmetric stretching vibration of CH_3, the stretching vibration of C=O, the symmetric bending vibration of CH_3, and the asymmetric stretching vibration of C–O–C, respectively.

The FT-IR spectra of the solution samples show that, with increasing lactide feed, the characteristic band of PBAT gradually decreases at 2958 cm^{-1}, while the PLA band becomes more prominent at 2995 cm^{-1}. Additionally, as the PLA band emerges at 1746 cm^{-1}, it begins to overlap with the PBAT carbonyl band at 1714 cm^{-1}. Other bands of PLA also become increasingly apparent at 1361 cm^{-1} and 1182 cm^{-1}. The spectra of melt samples look similar to those of solution samples. When comparing samples with the same lactide feed ratio, S1 and M1 display nearly identical spectra. However, noticeable differences are observed between S0.3 and M0.3. While specific bands of PLA are barely visible in the spectrum of S0.3, M0.3 shows distinct PLA bands at 1746 cm^{-1} and 1182 cm^{-1}. The disappearance of end-group signals in the ^{1}H-NMR spectrum of S0.3 indicates that lactide was successfully initiated at the PBAT chain end. Nevertheless, the FT-IR result of S0.3 suggests that the PLA segment did not grow significantly, which is consistent with the low ratio of lactide unit reported in Table 4. Although the IR spectrum of M0.3 clearly exhibits the specific bands of PLA, these bands cannot be attributed solely to the PLA segment within the block copolymer.

Tables 5 and 6 present the GPC results of the solution and melt samples, respectively. During the preparation of the solution samples, unreacted monomers were removed through precipitation. In contrast, the melt samples may retain residual monomers. Since these residual monomers can contaminate the GPC columns, the melt samples were dissolved in chloroform and precipitated into cold ethanol (4 °C). The precipitates were then collected and dried in a vacuum oven at 50 °C to obtain monomer-free samples. It should be noted, however, that when the melt samples were incorporated into PLA/PBAT blends, they were applied without this purification step.

In the case of the solution samples, S0.3 exhibited a number-average molar mass that dropped to approximately 60% of that of the macro-initiator, whereas the other three samples maintained molar mass comparable to the macro-initiator. In

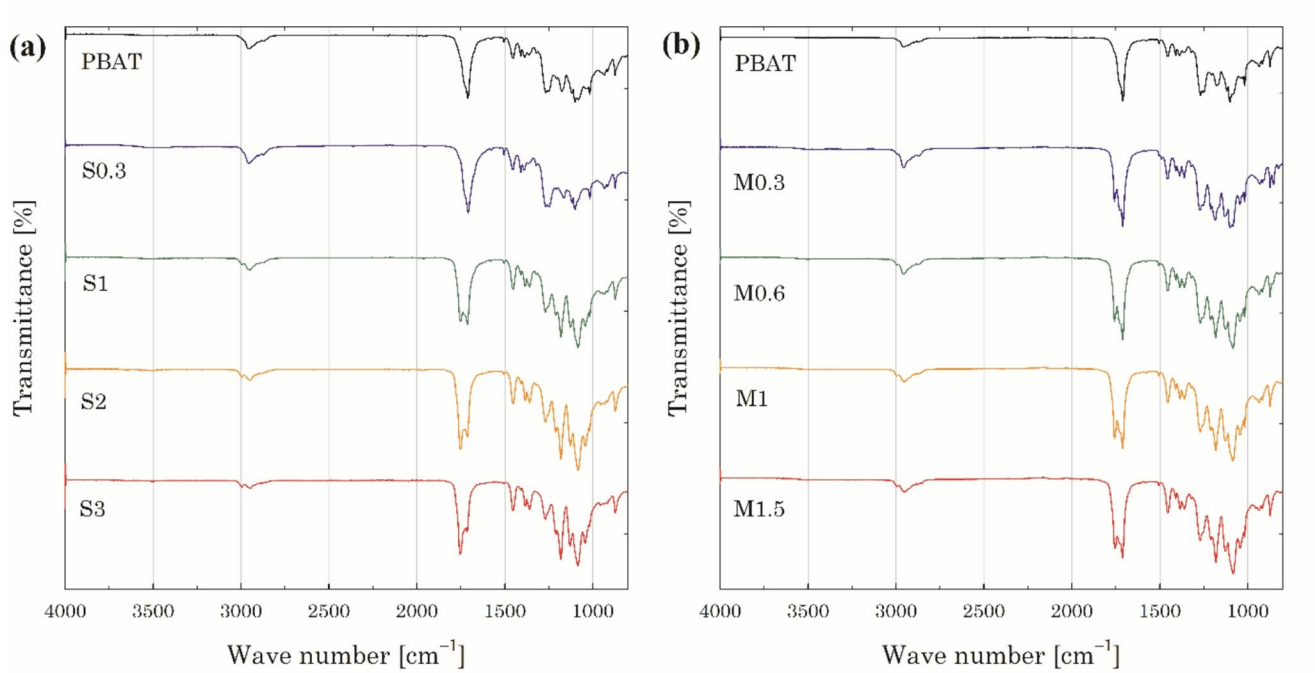

Fig. 2 FT-IR spectra of (a) solution samples and (b) melt samples, in comparison with the macro-initiator (PBAT)

Table 5 GPC results of the solution samples

Sample	M_n [g/mol]	M_w [g/mol]	Dispersity
S0.3	30,800	56,900	1.85
S1	61,600	132,000	2.14
S2	52,800	121,400	2.30
S3	57,900	124,600	2.15

Table 6 GPC results of the melt samples

Sample	M_n [g/mol]	M_w [g/mol]	Dispersity
M0.3	51,600	119,400	2.31
M0.6	52,100	126,500	2.43
M1	54,600	124,400	2.28
M1.5	60,500	139,300	2.30

contrast, all four melt samples retained molar mass similar to that of PBAT. Despite having the same lactide feed ratio as S0.3, M0.3 did not show a significant decrease in molar mass. Stannous octoate, a Lewis acid catalyst, not only initiates the ring-opening polymerization of lactide but also promotes the cleavage of ester bonds by coordinating with the carbonyl oxygen in PBAT [45]. These results seemed to indicate that the thermal degradation of PBAT appears to be more severe during the S0.3 polymerization than during the M0.3 polymerization. However, based on the NMR and GPC results, the apparent molar masses of PBAT were calculated to be 26,300 g/mol for S0.3 and 27,300 g/mol for M0.3, which are nearly identical.

Among the remaining three solution samples, S1 exhibited the highest weight-average molar mass and a relatively narrow dispersity in molar mass, indicating that the polymerization proceeded most uniformly in this sample. In contrast, S2 showed the lowest molar mass and the highest dispersity, suggesting that its polymerization was relatively less uniform. The molar mass of S3 was comparable to that of S1. Sedush and Chvalun [46] investigated the kinetics of $_L$-lactide polymerization using DSC by varying the concentration of stannous octoate and the reaction temperature. At 190 °C with 500 ppm of stannous octoate, an initial acceleration stage in the conversion rate was observed. However, at a catalyst concentration of 830 ppm, the conversion was so fast that the initial acceleration period was no longer distinguishable. Moreover, stannous octoate exhibited high catalytic activity even at low temperatures (e.g., 120 °C), and the occurrence of transesterification led to the formation of polymers with much higher molar mass than those obtained using other catalysts [47]. Wu et al. [48] reported that, in the ring-opening polymerization of ε-caprolactone using stannous octoate, an increase in monomer concentration led to a rise in the viscosity of the system, which consequently restricted the diffusion of monomers and resulted in a lower conversion. Although the solution polymerization in this study was carried out at a relatively low temperature of 130 °C, the catalyst concentration was as high as 5000 ppm (0.5 wt%), which is more than six times the concentration used in Sedush and Chvalun's study [46]. Therefore, the polymerization rate was expected to be very high at the beginning of the reaction. Given that a commercial high-molar-mass polymer was used as the macro-initiator, the system may

have experienced even more pronounced viscosity buildup with increasing monomer content.

The deterioration of quality in S2 is thought to have resulted from a localized increase in viscosity, which likely led to reduced mixing efficiency and reaction uniformity. In the experiment by Wu et al. [48], the restriction of monomer diffusion merely led to a decrease in monomer conversion. In our system using a macro-initiator, a shortage of available monomer may have enhanced chain scission of PBAT by stannous octoate, ultimately resulting in a reduction in the overall molar mass of the final polymer. This may explain why the molar mass of S2 is lower than that of S1. On the other hand, a much larger amount of monomer was introduced in S3. The presence of excess molten monomer may have buffered the rise in viscosity within the reaction system, thereby allowing monomer diffusion to recover. As a result, both the average molar mass and the dispersity in molar mass appear to have returned to levels comparable to those of S1. This interpretation remains tentative and would require further investigation.

At first glance, the GPC results in Table 5 may appear to conflict with the NMR analysis in Table 4; however, this is not the case. Table 5 represents the molar mass of the block copolymer, whereas Table 4 reflects the relative DP of each segment. As demonstrated in the case of S0.3, both the ring-opening polymerization of lactide and the chain scission of PBAT occur simultaneously in this system. Therefore, an increase in the DP of the PLA segment does not necessarily correspond to an increase in the molar mass of the block copolymer.

In contrast to the solution samples, the molar mass of the melt samples increased consistently with higher lactide feed ratios. Since the initiating sites are limited to the hydroxyl end groups of PBAT in solution polymerization, changes in the accessibility of monomer may influence the molar mass characteristics of the resulting polymer. In contrast, in melt polymerization, the presence of additional initiating sites—such as moisture—enables the increased lactide content to contribute more directly to the growth of molar mass.

The studies by Sun et al. [32] and Ding et al. [43] on PLA–PBAT–PLA triblock copolymers discussed the consistency between the DP determined by NMR and the molar mass measured by GPC. In both cases, PBAT with hydroxyl groups at both chain ends was synthesized and used as a macro-initiator to prepare triblock copolymers. However, since PBAT is a condensation-type polymer, achieving high molar mass is inherently challenging. Although the PBAT used in both studies was synthesized via melt polycondensation, its number-average molar mass was only about one-sixth to one-third that of the commercial PBAT (PBG7070) used in this study. As the DP increases, the peak intensity of the end-group in the NMR spectrum becomes weaker, making it difficult to reliably determine the DP determined by NMR. Therefore, in this study, which employed commercial PBAT as the macro-initiator, the comparison between the molar mass obtained from GPC and those estimated from NMR was omitted.

Figure 3 shows the DSC thermograms of the solution and melt samples. PBAT typically exhibits a glass transition temperature (T_g) at around −30 °C and a melting temperature (T_m) at approximately 130 °C, whereas PLA shows T_g and T_m at about 60 °C and 170 °C, respectively. In addition, a cold crystallization temperature (T_{cc}) is observed between 100 and 130 °C in the thermogram of PLA. S0.3 exhibited only a T_m of 127 °C, nearly identical to that of the PBAT macro-initiator, while the other solution samples showed distinct thermal transitions (T_g, T_{cc}, and T_m) different from PBAT. As in the results in Fig. 2; Table 4, the DSC thermogram of S0.3 indicated that the PLA segment did not sufficiently grow during polymerization.

In the other three samples, the T_m and T_g appeared at similar positions. However, T_{cc} showed significant variation: in S1, T_{cc} appeared at 125 °C, which is approximately 50 °C higher than that observed in S2 and S3 (78 °C). This suggests that crystallization is much more difficult for the PLA segment in S1 than for those in S2 or S3. This difference can be interpreted in light of the DP ratio of both segments (Table 4) and the overall molar mass of the block copolymer (Table 5). Although S1 and S3 exhibited similar molar masses, the DP ratio of the PLA segment to the PBAT segment in S3 was approximately three times higher than that in S1. This implies that the PBAT segment in S1 is significantly longer than in S3. For example, if both segments in S1 have a DP of 30 and the PLA and PBAT segments in S3 have DPs of 90 and 10, respectively, the DP ratio of S3 is three times that of S1. Given the molar masses of the repeating units of PLA (72 g/mol) and PBAT (estimated at 210 g/mol as the average of BT and BA units), the calculated total molar masses of S1 and S3 are approximately 8,460 g/mol and 8,680 g/mol, respectively, indicating that they are nearly identical. Based on this example, the thermal behavior in Fig. 3 can be explained as follows: In S1, the comparable lengths of the PLA and PBAT segments suggest that the PBAT segment interferes with the crystallization of the PLA segment. In contrast, the significantly shorter PBAT segment in S3 allows the PLA segment to remain more flexible, thereby promoting faster crystallization. Therefore, the T_{cc} peak of S3 appears at a lower temperature and with a larger area than that of S1.

Unlike the solution samples, the melt samples exhibit two distinct endothermic peaks corresponding to cold crystallization. One appears relatively sharp and at a temperature similar to the T_{cc} of the solution samples, while the other is broader and observed near 130 °C. As the lactide

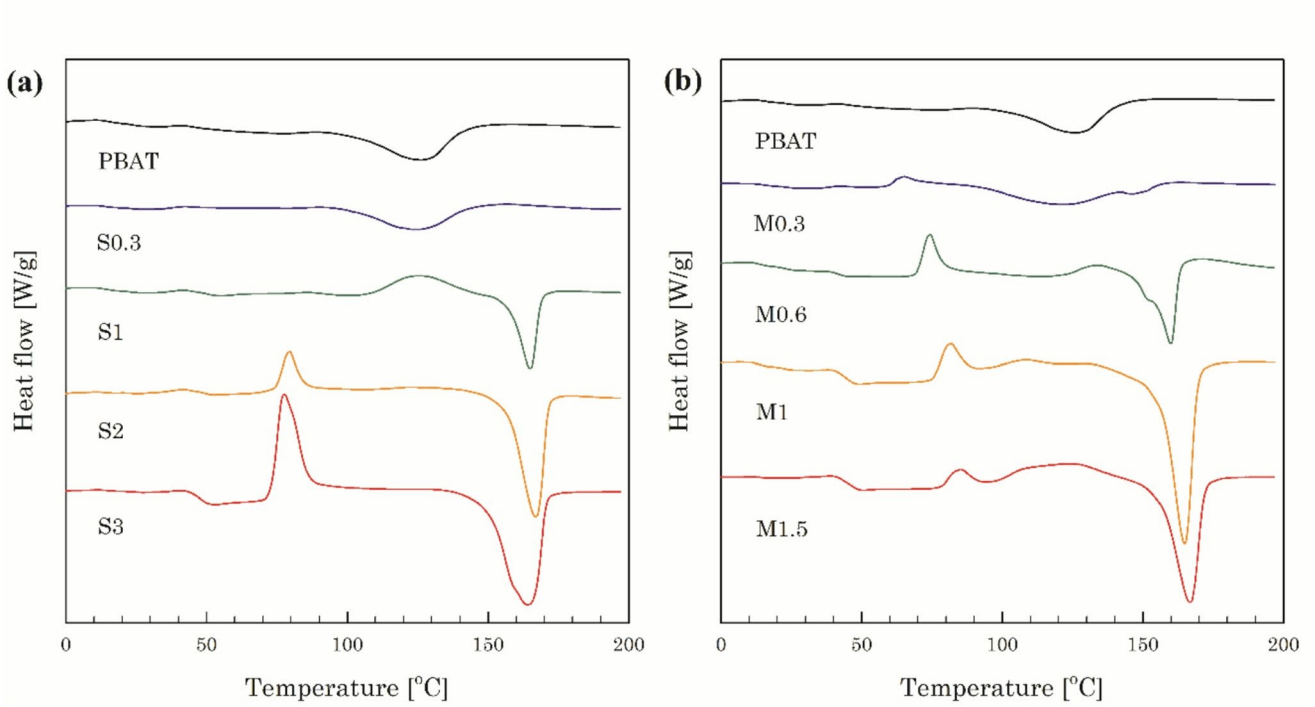

Fig. 3 DSC thermograms of (a) solution samples and (b) melt samples, in comparison with the macro-initiator (PBAT)

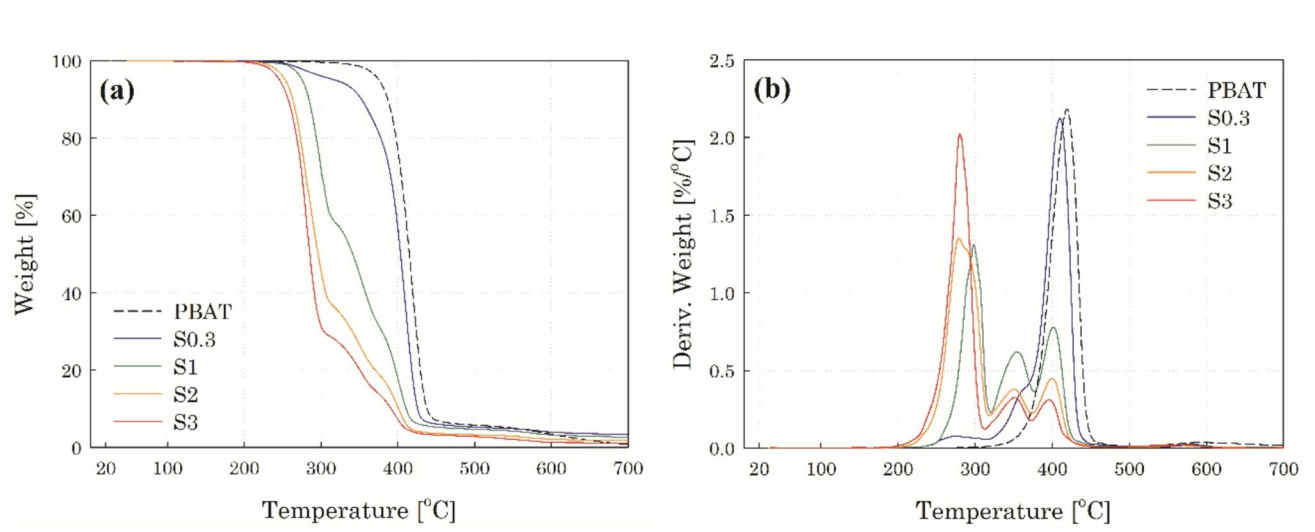

Fig. 4 (a) TGA and (b) DTA curves of solution samples, in comparison with the macro-initiator (PBAT)

feed ratio increases, the low-temperature peak shifts to higher temperatures with little change in peak area, whereas the high-temperature peak becomes more pronounced and increases in area. The low-temperature peak is presumed to correspond to the crystallization behavior of PLA segments in the block copolymer. In contrast, the high-temperature peak—whose area increases with higher lactide content—is likely attributable to the crystallization of PLA homopolymers. The gradual shift of the low-temperature peak with increasing lactide feed ratio suggests that the presence of PLA homopolymers may interfere with or delay the crystallization of PLA segments in the block copolymer.

Figure 4 presents the TGA and DTA curves of the solution samples, and Table 7 summarizes the thermal decomposition temperatures and corresponding weight losses for each decomposition step. In polymer blends, when the constituent polymers have sufficiently different decomposition temperatures and undergo independent single-step decomposition, the number of weight-loss steps observed in TGA typically corresponds to the number of components.

Table 7 Thermal decomposition temperatures and corresponding weight losses at each decomposition step

Sample	Step 1		Step 2		Step 3	
	℃	%	℃	%	℃	%
S0.3	275.4	4.7	-	-	410.1	89.1
S1	298.3	42.1	355.1	26.7	401.4	25.9
S2	279.0	61.6	350.5	15.0	399.8	19.7
S3	280.0	69.1	351.0	13.6	395.9	14.0

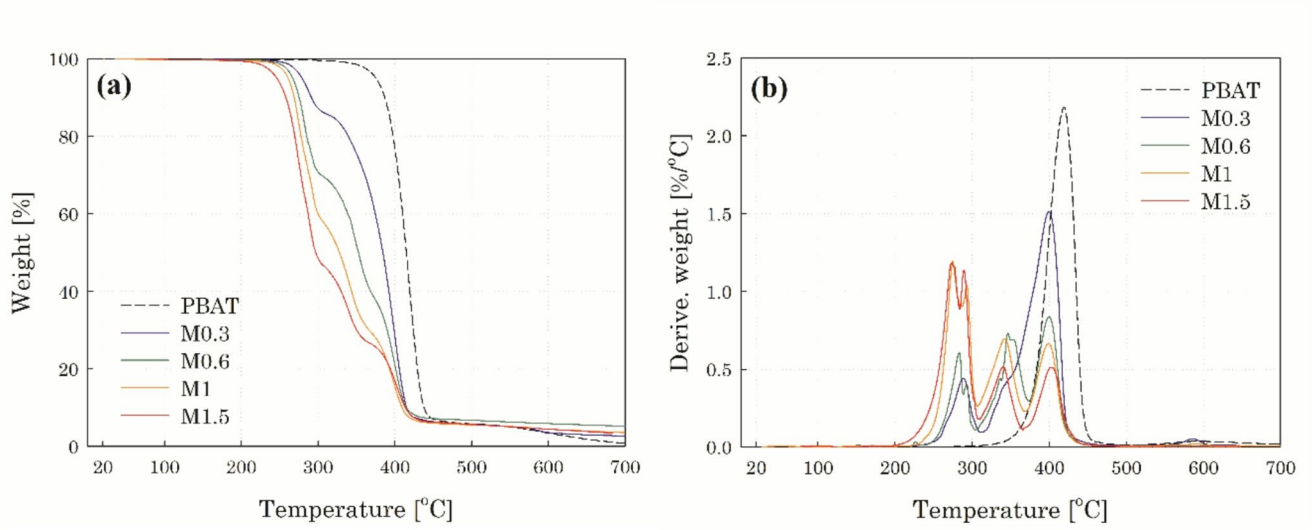

Fig. 5 (a) TGA and (b) DTA curves of melt samples, in comparison with the macro-initiator (PBAT)

However, since the two segments in block copolymers are covalently bonded, their thermal decomposition behaviors are unlikely to proceed independently. All solution samples except S0.3 exhibit a three-step decomposition profile. Unfortunately, the studies by Sun et al. [32] and Ding et al. [43], which investigated PLA–PBAT–PLA triblock copolymers, did not report TGA data.

Báez et al. [49] reported a case where a diblock copolymer exhibited multi-step thermal decomposition behavior. They synthesized a poly(ethylene-*b*-ε-caprolactone) (PE-*b*-PCL) diblock copolymer by ring-opening polymerization of ε-caprolactone using polyethylene with hydroxyl end groups (PE–OH) as a macro-initiator. Even though the thermal decomposition temperatures of the two homopolymers—PE (369 °C) and PCL (364 °C)—were quite close, the block copolymer exhibited a distinct multi-step decomposition profile. When the feed ratio of PE to PCL in the block copolymer was 65:35, thermal decomposition occurred in three distinct steps (309 °C, 362 °C, and 430 °C), and four decomposition steps were observed at a PE: PCL ratio of 25:75. As the PCL content increased, thermal stability decreased, the decomposition occurred over a broader temperature range, and the number of decomposition steps increased. They assigned each decomposition step to the corresponding block, based on the changes in peak intensity associated with block composition.

The segmental DP ratios listed in Table 3 correspond to PLA-to-PBAT weight ratios of 0.75, 1.82, and 2.68 for samples S1, S2, and S3, respectively. Since the decomposition proceeds in three distinct steps, it can be inferred that one of the two segments undergoes two different decomposition mechanisms. Assuming that step 1 corresponds to the decomposition of the PLA segment and steps 2 and 3 to that of the PBAT segment, the PLA-to-PBAT weight ratios calculated from Table 5 (0.80, 1.78, and 2.51 for S1, S2, and S3, respectively) are in good agreement with those obtained from the NMR analysis. It should be noted that this assignment is made under the assumption that each step corresponds to only one segment. To go beyond this assumption and elucidate the decomposition mechanisms more accurately, further analysis using pyrolysis-gas chromatography/mass spectrometry (Py-GC/MS) is required [50].

The TGA and DTA profiles of the melt samples are displayed in Fig. 5, and the corresponding decomposition temperatures and weight losses for each step are summarized in Table 8. Except for M0.3, all melt samples exhibited a three-step thermal decomposition profile, which is consistent with the behavior observed in the solution samples. However, the first decomposition step of the melt samples differed notably from that of the solution samples: although it appeared as a single peak, the apex was split into two closely spaced subpeaks, indicating peak overlap. Even in the case of M0.3,

Table 8 Thermal decomposition temperatures and corresponding weight losses at each decomposition step

Sample	Step 1		Step 2		Step 3	
	°C	%	°C	%	°C	%
M0.3	288.6	14.3	-	-	399.7	79.7
M0.6	283.5, 293.5	29.9	346.4	31.7	399.7	31.4
M1	274.5, 293.0	42.1	341.8	28.3	399.0	23.9
M1.5	273.3, 289.2	53.6	340.3	19.5	401.9	20.9

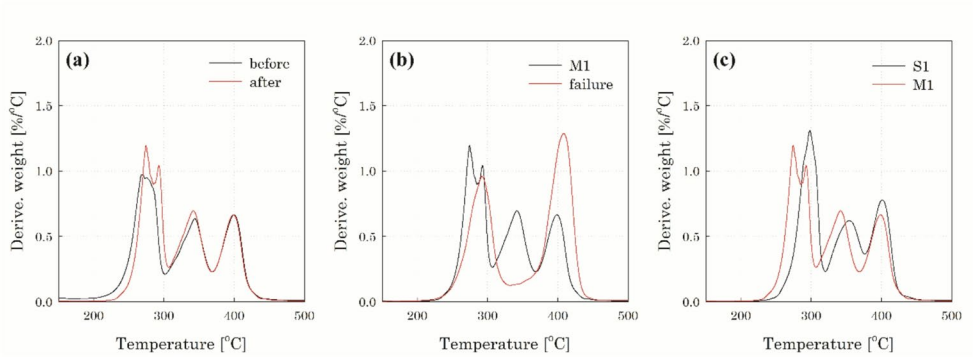

Fig. 6 Comparison of the DTA thermograms of M1 to (a) the unpurified M1, (b) the sample in which block copolymerization failed, and (c) S1, the solution sample prepared with the same lactide feed ratio

which did not exhibit a three-step decomposition profile, the first DTA peak was sharper and more distinct than that of S0.3. It should be noted that the thermograms in Fig. 5 were obtained from purified samples after the removal of residual monomers. Figure 6(a) compares the DTA curves of M1 before and after purification. When unreacted monomers remained in the sample, the split apex in the first decomposition step was not observed, suggesting that the presence of residual monomers reduces the thermal stability and obscures this feature.

The DTA curve of the solution sample (S1) exhibited three peaks. Based on the analysis summarized in Table 5, we confirmed that the first thermal decomposition step corresponds to the decomposition of PLA (either PLA segments or PLA homopolymer), whereas the second and third steps are attributable to the decomposition of PBAT. However, in the case of the melt sample (M1) (Fig. 6(a)), the first decomposition peak appeared to split into two apexes. This raised the question of which of the two apexes corresponds to the PLA segment in the block copolymer. To elucidate this matter, we executed an extreme experimental scenario by deliberately introducing water into the reactor to ascertain the location of the thermal decomposition peak associated with PLA homopolymer in the DTA thermogram (Fig. 6(b)). The second decomposition step was not observed in the failure case, which means that it corresponds to the decomposition of the PBAT segment. Moreover, the first decomposition peak of the failure case appeared at a temperature nearly identical to that of the higher-temperature apex in the first decomposition step of M1. This suggests that the lower-temperature apex in M1 corresponds to the thermal decomposition of the PLA segment in the block copolymer. As shown in Tables 5 and 6, the melt samples exhibited slightly broader dispersity in molar mass than the solution samples, which was reflected in the GPC curves merely as a change in peak width. In contrast, the DTA curve clearly separates the thermal decomposition contributions of the PLA homopolymer and the PLA block, providing more detailed insight into the PLA component.

Figure 6(c) compares the DTA curves of M1 and S1, synthesized with the same lactide feed ratio using different polymerization methods. Based on the interpretation in Fig. 6(b), the lower-temperature apex of the first decomposition step in M1 was attributed to the thermal decomposition of the PLA segment in the block copolymer. Accordingly, this apex was used to determine the first-step decomposition temperature of M1. The temperature differences between M1 and S1 were 25 °C, 13 °C, and 2 °C for the first, second, and third decomposition steps, respectively. Although both samples follow a similar three-step decomposition profile, M1 is markedly less thermally stable than S1 in the first two steps. Low-molar-mass PLA, which is commonly used as a plasticizer for PLA resins, is also known to affect their thermal stability. Burgos et al. [51] reported that the addition of 15 wt% of oligomeric lactic acid to PLA resin reduced the initial decomposition temperature (T_5) by 60 °C. It is assumed that the PLA homopolymer, formed concurrently during polymerization, is poorly miscible with PBAT and is therefore encapsulated by the PLA-PBAT block copolymer, forming a shell-like structure within the matrix. Accordingly, the presence of PLA homopolymer (or oligomer) appears to exert the most pronounced influence on the first decomposition step, which corresponds to the thermal decomposition of the PLA segment. Furthermore, among the two decomposition steps of PBAT, the second step—where a significant reduction in thermal stability was observed—is likely

associated with the PBAT segment whose decomposition behavior is not independent of the PLA segment.

Assuming that step 1 corresponds to the decomposition of the PLA component and steps 2 and 3 to the decomposition of the PBAT component, the PLA-to-PBAT weight ratios of the melt samples were calculated to be 0.18, 0.47, 0.81, and 1.33 for M0.3, M0.6, M1, and M1.5, respectively. Although M1 and S1 show similar PLA-to-PBAT weight ratios due to the same lactide feed ratio, the ratio for M1—as inferred from Fig. 6—reflects the combined weight of the PLA homopolymer and the PLA segment within the block copolymer.

Comparison of Blends Incorporating Block Copolymers Via Different Polymerization

Figure 7 presents the elongation at break and tensile strength of PLA/PBAT blends containing the solution samples, expressed as ratios relative to those of the pristine blend. S0.3, which exhibited a significant reduction in molar mass, resulted in decreases in both tensile strength and elongation at break. The improvement in tensile strength was comparable when either S1 or S3 was used. However, in terms of elongation at break, S1 proved more effective than S3. According to the results of NMR and GPC analyses, S1 and S3 exhibited similar overall molar mass; however, the DP of the PLA segment relative to the PBAT segment was approximately 3.6 times higher in S3 than in S1. This suggests that the PBAT segment in S1 has a higher DP than that in S3. Although commercial PBAT was used as the macroinitiator, chain scission of PBAT can occur under certain polymerization conditions, as previously discussed. The higher elongation at break observed in the blend containing S1 is therefore attributed to the longer PBAT segment, which likely imparts greater flexibility and toughness to the system.

Sun et al. [32] reported that the addition of block copolymer above 2 wt% did not result in further improvement in compatibility. However, in the present study, enhancements in mechanical properties—attributed to improved compatibility—were observed even at block copolymer contents up to 8 wt%. This discrepancy may be attributed to differences in blend composition. While Sun et al. [32] used a PLA/PBAT ratio of 80:20, the present study employed a ratio of 45:55. According to Jang et al. [52], a co-continuous morphology is typically observed in PLA/PBAT blends when the PLA content ranges from 35 wt% to 65 wt%. In such morphologies, the interfacial area is significantly increased, thereby necessitating a greater amount of block copolymer to stabilize the interface.

Figure 8 presents the elongation at break and tensile strength of PLA/PBAT blends incorporating melt samples, expressed as ratios relative to those of the pristine blend. All melt samples except M0.3 improved the tensile strength of the blends, whereas elongation at break increased in all blends regardless of the melt sample used. For both properties, the extent of improvement became more pronounced with increasing lactide feed ratio. When the content of block

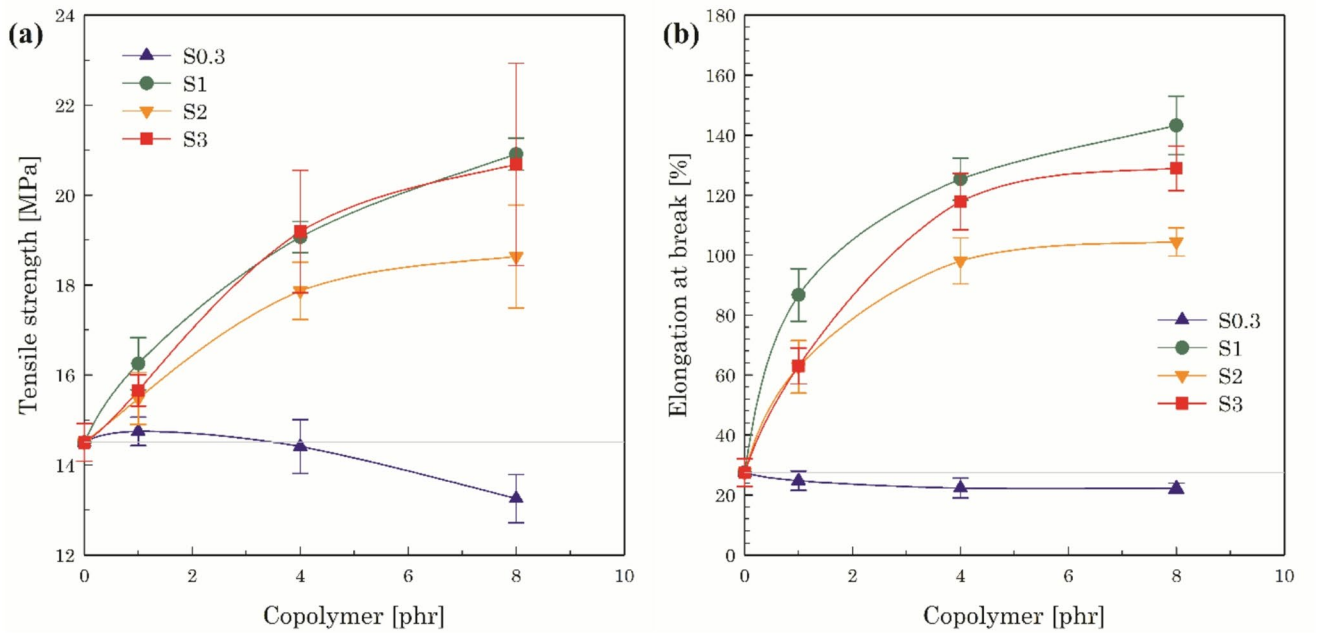

Fig. 7 Mechanical properties of PLA/PBAT blends containing solution samples as compatibilizers: (a) tensile strength and (b) elongation at break, expressed as ratios relative to those of the pristine blend

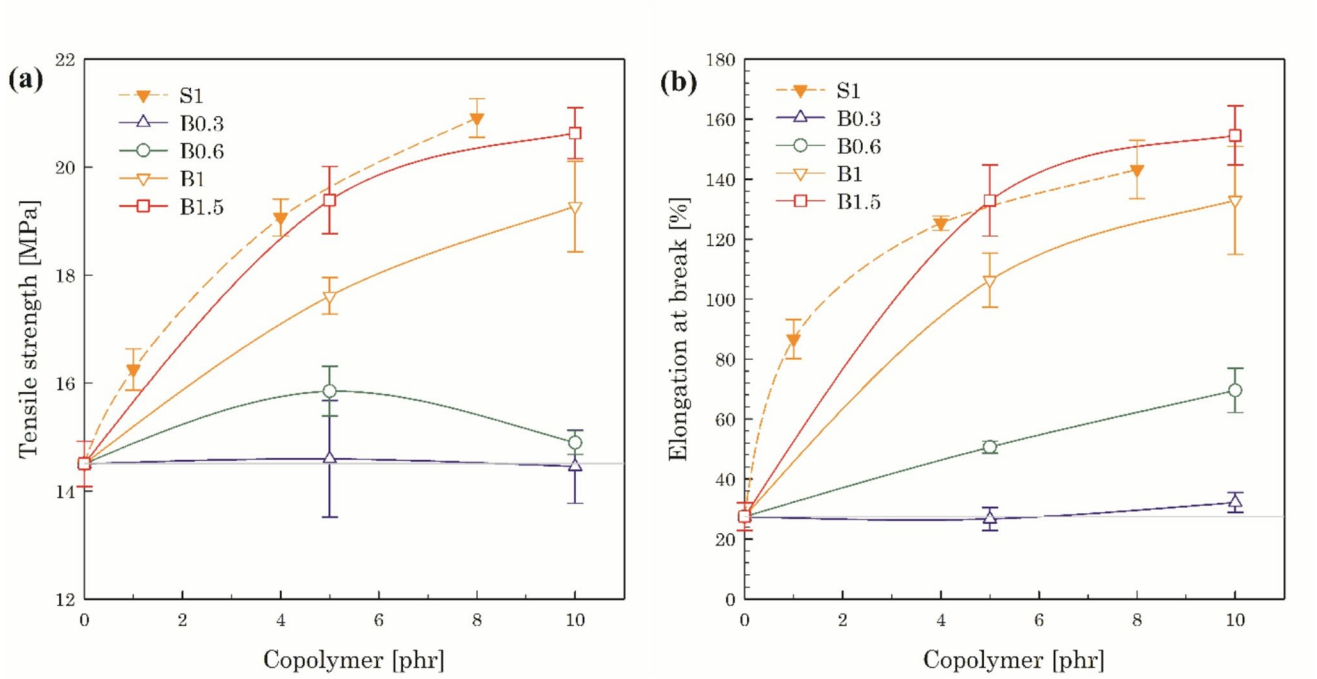

Fig. 8 Mechanical properties of PLA/PBAT blends containing melt samples as compatibilizers: (a) tensile strength and (b) elongation at break, expressed as ratios relative to those of the pristine blend, with the dashed line representing the blend containing the solution sample S1, which exhibited the most significant compatibilization effect

copolymer was 5 phr or less, M1.5 exhibited a comparable improvement in tensile strength to that of S1. This suggested that although the melt sample is less efficient than the solution sample, its lower efficiency could be offset by increasing the lactide feed ratio. When the content of block copolymer exceeds a certain threshold, the rate of increase in tensile strength begins to diminish in both blends containing the solution sample and those containing the melt sample. Notably, in the case of M0.6, the tensile strength at 10 phr was lower than that at 5 phr. A similar reduction in the slope of the tensile strength curve was observed in both M1.5- and S1-containing blends beyond 5 phr, with a more pronounced decline in the blend with M1.5. This suggests that M1.5 cannot replace S1 effectively at contents above 5 phr.

Figure 9 presents the SEM micrographs of PLA/PBAT blends with and without block copolymer (S1 or M1), together with the variation in droplet size as a function of the amount of block copolymer. The upper part shows blends containing S1 at 4 and 8 phr, while the lower part displays blends containing M1 at 5 and 10 phr. In the pristine blend, dispersed domains appear in droplet-like form, but the irregularity in their size and shape suggests the onset of a co-continuous structure. For both S1- and M1-containing blends, the domain size decreased progressively with increasing the content of block copolymer. This reduction in domain size indicates the potential for enhanced compatibility between PLA and PBAT. Nevertheless, despite the higher content of M1 (5 and 10 phr) compared to S1 (4 and 8 phr), the dispersed domains were relatively smaller in the blends containing S1, indicating that the solution sample was more effective in reducing domain size than the melt sample.

Figure 10 shows the DSC thermograms of PLA/PBAT blends containing 5 or 10 phr of melt samples, compared with the pristine PLA/PBAT blend. In the pristine blend, the melting peak of PBAT appears broadly at 114 °C, while that of PLA is observed sharply at 150 °C. Upon addition of the 5 phr melt sample, a cold crystallization peak of PLA emerges between 110 and 130 °C, and a small shoulder peak appears on the higher-temperature side of the PLA melting peak in the case of M1 and M1.5. When the amount of melt samples is increased to 10 phr, two distinct melting endotherms at 150 °C and 160 °C are clearly observed in blends containing M1 and M1.5.

As shown in Fig. 3(b), the melt samples showed two different T_{cc}. We attributed the higher-temperature T_{cc} to the crystallization of PLA homopolymer and the lower-temperature T_{cc} to the crystallization of PLA segments in the block copolymer, given that the solution samples showed a single T_{cc} around 78 °C and that the area of the higher-temperature T_{cc} increased with the lactide feed ratio. According to Tábi et al. [53], when crystallization occurs between 100 and 120 °C, both α′ and α crystal forms of PLA can be generated, while crystallization above 120 °C results only in

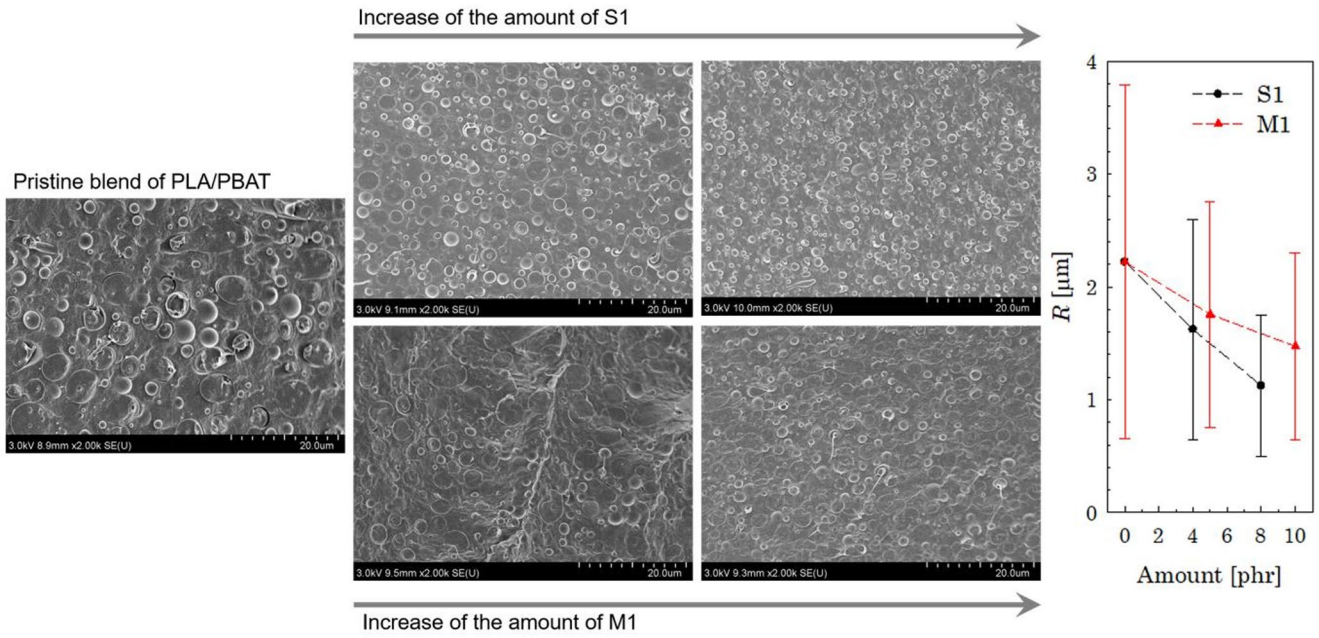

Fig. 9 SEM images of the pristine PLA/PBAT blend and blends compatibilized with varying amounts of S1 or M1, together with the variation in droplet size as a function of the amount of compatibilizers

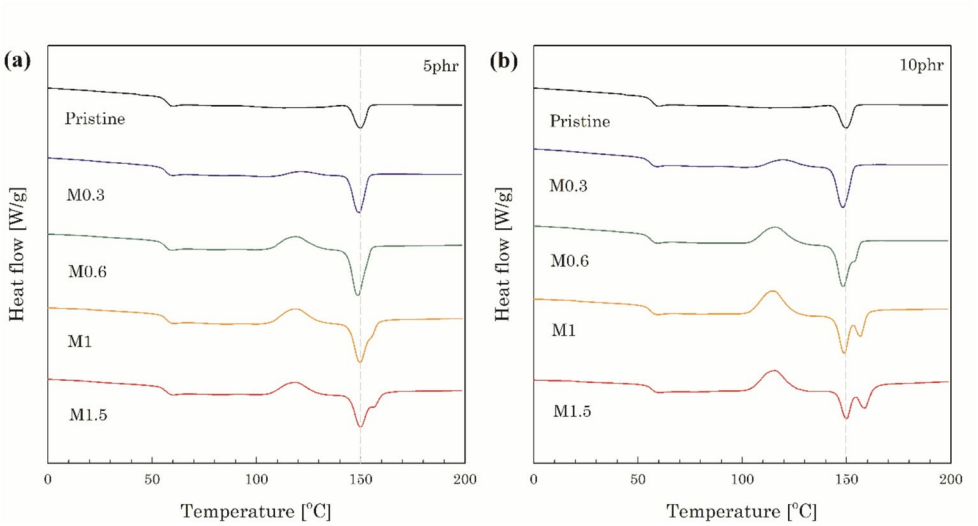

Fig. 10 DSC thermograms of PLA/PBAT blends containing (a) 5 phr or (b) 10 phr of melt samples, compared with the pristine PLA/PBAT blend

the stable α form of PLA. In Fig. 3(b), melt samples with higher lactide feed ratios exhibited a broad higher-temperature T_{cc} between 100 and 140 °C, suggesting that the PLA homopolymer predominantly formed the stable α crystalline structure. Therefore, upon incorporation of the melt samples into PLA/PBAT blends, the PLA homopolymer present in the melt samples seemed to serve as a nucleating agent, facilitating the crystallization of the PLA component into the stable α form.

In summary, the pristine blend exhibited a PLA melting peak at 150 °C originating from the relatively metastable α′ crystal form. In contrast, the blends containing melt samples showed the coexistence of both α and α′ crystals. The α form seemed to be increasingly dominant as the lactide feed ratio in the melt sample increased. However, the transformation of the crystalline structure of PLA from the α′ to the α form is a structural change confined to the PLA domains themselves and thus does not directly affect PLA–PBAT miscibility or intensify phase separation. Nevertheless, this transition yields a more stable and compact crystalline structure, which can influence the overall blend morphology. According to Jang et al. [52], a PLA/PBAT blend with a 45:55 ratio lies within the composition range that exhibits a co-continuous morphology. However, the densification resulting from the transformation of the PLA crystals may cause irregular co-continuous droplets to develop into

domains with sharper boundaries and well-defined interfaces in PBAT-rich blends.

When the crystalline structure of PLA in the blend transforms into a stable form, improvements in mechanical strength, thermal stability, and dimensional stability can be expected. Nevertheless, the increase in tensile strength shown in Fig. 9(a) upon the incorporation of melt samples may raise the suspicion that this effect originates solely from the enhanced strength of the PLA component. If the improvement were merely attributable to the crystalline transformation of PLA, however, the elongation at break would be expected to decrease upon the addition of melt samples. In contrast, the blends containing melt samples exhibited a gradual increase in elongation at break along with tensile strength, as shown in Fig. 9(b). This suggests that the melt samples—comprising both block copolymers and PLA homopolymers—not only promote the crystalline transformation of PLA but also enhance the compatibility between the two blend components. To clearly distinguish the contribution of interfacial adhesion from that of crystalline transformation to the improvement in tensile strength, further investigation of viscoelastic properties would be required to directly assess interfacial property. Moreover, it should be recognized that the emergence of an additional melting peak necessitates higher processing temperatures, which may act as a drawback from a processing perspective.

Conclusion

In this study, PLA–PBAT block copolymers were synthesized using commercial PBAT as a macro-initiator through two distinct methods: conventional solution polymerization and melt polymerization, the latter serving as a precursor to reactive extrusion. By varying the lactide feed ratio, we compared the properties of the resulting copolymers and their performance in the improvement of tensile properties of PLA/PBAT blends.

Owing to the metallic structure of the internal mixer used for melt polymerization, ambient moisture inevitably entered the reaction chamber. As a result, unlike the solution samples, the melt samples contained both block copolymers and PLA homopolymers. Since the commercial PBAT with a high molar mass was used as a macro-initiator, we initially expected to observe a clear distinction between the two products in GPC analysis, such as a shift or splitting in the elution curves. However, both products exhibited a single broad elution peak, with the melt samples displaying a slightly broader distribution.

Notably, the differences between the two samples were more clearly discerned in the DTA curves. The PLA–PBAT block copolymers exhibited a three-step thermal decomposition behavior in TGA, with the first step corresponding to the decomposition of the PLA segment. Each step produced a distinct peak in the DTA curve. In contrast to the solution samples, the melt samples showed a split apex in the first DTA peak, indicating the coexistence of two types of PLA chains—PLA segments in the block copolymer and PLA homopolymer. Such characteristics can be used as a tool to comparatively evaluate the fraction of PLA homopolymer in the melt samples by representing the intensity of the two apexes in terms of their ratio.

For the melt samples, the tensile properties increased gradually with increasing lactide feed ratios, and all the samples had the molar mass comparable to that of the macro-initiator. In contrast, the solution samples did not show a clear trend in molar mass or compatibilization efficiency. Moreover, the robustness of melt polymerization can help maintain the quality of the block copolymer when used as an additive. The solution sample, which consists predominantly of block copolymers, improved the mechanical properties of PLA/PBAT blends more than the melt sample. However, the blend incorporated by M1.5 achieved tensile strength comparable to that of S1 under a certain concentration. This result suggests that increasing the lactide feed ratio in melt polymerization can partially offset the performance limitations caused by the presence of homopolymers.

Author Contributions M. K. Kwon prepared the samples, interpreted the data, and wrote the original draft of the manuscript. Y. J. Lee performed the instrumental analyses, contributed to data validation, and reviewed the manuscript. S. G. Lee designed the experiments and edited the manuscript. S. G. Kim helped with the experiments and reviewed the manuscript in a viewpoint of industrial application. S. J. Lee supervised the overall research and provided a critical review of the manuscript as a corresponding author.

Funding Open Access funding enabled and organized by DGIST (Daegu Gyeongbuk Institute of Science & Technology). This work was supported by the DGIST R&D Program of the Ministry of Science, ICT and Future Planning of Korea (25-NT-01). It was also supported by the Strategy Technology Development Programs of the Ministry of Trade, Industry & Energy of Korea (RS-2024-00433459).

Data Availability No datasets were generated or analysed during the current study.

Declarations

Competing Interests The authors declare no competing interests.

References

1. Jiang L, Wolcott MP, Zhang J (2006) Study of biodegradable polylactide/poly(butylene adipate-*co*-terephthalate) blends. Biomacromolecules 7(1):199–207. https://doi.org/10.1021/bm050581q
2. Yeh J-T, Tsou C-H, Huang C-Y, Chen K-N, Wu C-S, Chai W-L (2010) Compatible and crystallization properties of poly(lactic acid)/poly(butylene adipate-*co*-terephthalate) blends. J Appl Polym Sci 116(2):680–687. https://doi.org/10.1002/app.30907
3. Aversa C, Barletta M, Cappiello G, Gisario A (2022) Compatibilization strategies and analysis of morphological features of poly(butylene adipate-*co*-terephthalate) (PBAT)/poly(lactic acid) PLA blends: a state-of-art review. Eur Polym J 173:111304. https://doi.org/10.1016/j.eurpolymj.2022.111304
4. Self JL, Zervoudakis AJ, Peng X, Lenart WR, Macosko CW, Ellison CJ (2022) Linear, graft, and beyond: multiblock copolymers as next-generation compatibilizers. JACS Au 2(2):310–321. https://doi.org/10.1021/jacsau.1c00500
5. Duan H, Shang X, Wu X, Ma L, Xing C, Zhu J (2025) Epoxy-based chain extenders in polylactic acid (PLA): a comprehensive review of structure, performance, and challenges. J Mater Sci Chem Eng 13(1):20–44. https://doi.org/10.4236/msce.2025.131003
6. Kumar M, Mohanty S, Nayak SK, Rahail Parvaiz M (2010) Effect of glycidyl methacrylate (GMA) on the thermal, mechanical and morphological property of biodegradable PLA/PBAT blend and its nanocomposites. Bioresour Technol 101(21):8406–8415. https://doi.org/10.1016/j.biortech.2010.05.075
7. Zhang N, Wang Q, Ren J, Wang L (2009) Preparation and properties of biodegradable poly(lactic acid)/poly(butylene adipate-*co*-terephthalate) blend with glycidyl methacrylate as reactive processing agent. J Mater Sci 44:250–256. https://doi.org/10.1007/s10853-008-3049-4
8. Al-Itry R, Lamnawar K, Maazouz A (2012) Improvement of thermal stability, rheological and mechanical properties of PLA, PBAT and their blends by reactive extrusion with functionalized epoxy. Polym Degrad Stab 97(10):1898–1914. https://doi.org/10.1016/j.polymdegradstab.2012.06.028
9. Al-Itry R, Lamnawar K, Maazouz A (2014) Reactive extrusion of PLA, PBAT with a multi-functional epoxide: physico-chemical and rheological properties. Eur Polym J 58:90–102. https://doi.org/10.1016/j.eurpolymj.2014.06.013
10. Arruda LC, Magaton M, Bretas RES, Ueki MM (2015) Influence of chain extender on mechanical, thermal and morphological properties of blown films of PLA/PBAT blends. Polym Test 43:27–37. https://doi.org/10.1016/j.polymertesting.2015.02.005
11. Li X, Yan X, Yang J, Pan H, Gao G, Zhang H, Dong L (2018) Improvement of compatibility and mechanical properties of the poly(lactic acid)/poly(butylene adipate-*co*-terephthalate) blends and films by reactive extrusion with chain extender. Polym Eng Sci 58(10):1868–1878. https://doi.org/10.1002/pen.24795
12. Wang X, Peng S, Chen H, Yu X, Zhao X (2019) Mechanical properties, rheological behaviors, and phase morphologies of high-toughness PLA/PBAT blends by in-situ reactive compatibilization. Compos B Eng 173:107028. https://doi.org/10.1016/j.compositesb.2019.107028
13. Pan H, Li Z, Yang J, Li X, Ai X, Hao Y, Zhang H, Dong L (2018) The effect of MDI on the structure and mechanical properties of poly(lactic acid) and poly(butylene adipate-*co*-butylene terephthalate) blends. RSC Adv 8:4610–4623. https://doi.org/10.1039/C7RA10745E
14. Ma P, Cai X, Zhang Y, Wang S, Dong W, Chen M, Lemstra PJ (2014) In-situ compatibilization of poly(lactic acid) and poly(butylene adipate-*co*-terephthalate) blends by using dicumyl peroxide as a free-radical initiator. Polym Degrad Stab 102:145–151. https://doi.org/10.1016/j.polymdegradstab.2014.01.025
15. Signori F, Boggioni A, Righetti MC, Rondán CE, Bronco S, Ciardelli F (2015) Evidences of transesterification, chain branching and cross-linking in a biopolyester commercial blend upon reaction with dicumyl peroxide in the melt. Macromol Mater Eng 300(2):153–160. https://doi.org/10.1002/mame.201400187
16. Lu X, Zhao J, Yang X, Xiao P (2017) Morphology and properties of biodegradable poly (lactic acid)/poly (butylene adipate-*co*-terephthalate) blends with different viscosity ratio. Polym Test 60:58–67. https://doi.org/10.1016/j.polymertesting.2017.03.008
17. Coltelli M-B, Toncelli C, Ciardelli F, Bronco S (2011) Compatible blends of biorelated polyesters through catalytic transesterification in the melt. Polym Degrad Stab 96(5):982–990. https://doi.org/10.1016/j.polymdegradstab.2011.01.028
18. Lin S, Guo W, Chen C, Ma J, Wang B (2012) Mechanical properties and morphology of biodegradable poly(lactic acid)/poly(butylene adipate-*co*-terephthalate) blends compatibilized by transesterification. Mater Des (1980–2015) 36:604–608. https://doi.org/10.1016/j.matdes.2011.11.036
19. Nam K, Kim SG, Kim DY, Lee DY (2024) Enhanced mechanical properties of polylactic acid/poly(butylene adipate-*co*-terephthalate) modified with maleic anhydride. Polymers (Basel) 16(4):518. https://doi.org/10.3390/polym16040518
20. Liu C, Lin S, Zhou C, Yu W (2013) Influence of catalyst on transesterification between poly(lactic acid) and polycarbonate under flow field. Polymer 54(1):310–319. https://doi.org/10.1016/j.polymer.2012.11.047
21. Su S (2022) Compatibilization, processing and characterization of poly(butylene adipate terephthala-te)/polylactide (PBAT/PLA) blends. Mater Res Express 9(2):025308. https://doi.org/10.1088/2053-1591/ac55c7
22. Huang S, Bai L, Trifkovic M, Cheng X, Macosko CW (2016) Controlling the morphology of immiscible cocontinuous polymer blends via silica nanoparticles jammed at the interface. Macromolecules 49(10):3911–3918. https://doi.org/10.1021/acs.macromol.6b00212
23. Qiao H, Zheng B, Zhong G, Li Z, Cardinaels R, Moldenaers P, Lamnawar K, Maazouz A, Liu C, Zhang H (2023) Understanding the rheology of polymer–polymer interfaces covered with Janus nanoparticles: polymer blends versus particle sandwiched multilayers. Macromolecules 56(2):647–663. https://doi.org/10.1021/acs.macromol.2c01973
24. Gavgani JN, Goharpey F, Velankar S (2021) Interfacially compatibilized PI/PDMS blends with reduced octadecylamine-functionalized graphene oxide: morphological and rheological properties. Soft Matter 17:9670–9681. https://doi.org/10.1039/D1SM01057C
25. Stancik EJ, Kouhkan M, Fuller GG (2004) Coalescence of particle-laden fluid interfaces. Langmuir 20:90–94. https://doi.org/10.1021/la0356093
26. Bhattacharyya AR, Ghosh AK, Misra A (2003) Ionomer compatibilised PA6/EVA blends: mechanical properties and morphological characterisation. Polymer 44(5):1725–1732. https://doi.org/10.1016/S0032-3861(02)00802-9
27. Baouz T, Fellahi S (2005) Interfacial modification of high density polyethylene/glass fiber reinforced and non reinforced polyamide

66 blends. J Appl Polym Sci 98(4):1748–1760. https://doi.org/10.1002/app.22359
28. Shamsuri AA, Jamil SNA, Md., Abdan K (2021) A brief review on the influence of ionic liquids on the mechanical, thermal, and chemical properties of biodegradable polymer composites. Polymers (Basel) 13(16):2597. https://doi.org/10.3390/polym13162597
29. Lopes Pereira EC, Da Silva MECF, Pontes K, Soares BG (2019) Influence of protonic ionic liquid on the dispersion of carbon nanotube in PLA/EVA blends and blend compatibilization. Front Mater Sci 6:1–14. https://doi.org/10.3389/fmats.2019.00234
30. Gebbie MA, Dobbs HA, Valtiner M, Israelachvili JN (2015) Long-range electrostatic screening in ionic liquids. PNAS 112(24):7432–7437. https://doi.org/10.1073/pnas.1508366112
31. Zhao X, Zhou K, Zhong Y, Liu P, Li Z, Pan J, Long Y, Huang M, Brakat A, Zhu H (2021) Hydrophobic ionic liquid-in-polymer composites for ultrafast, linear response and highly sensitive humidity sensing. Nano Res 14:1202–1209. https://doi.org/10.1007/s12274-020-3172-3
32. Sun Z, Zhang B, Bian X, Feng L, Zhang H, Duan R, Sun J, Pang X, Chen W, Chen X (2015) Synergistic effect of PLA–PBAT–PLA tri-block copolymers with two molecular weights as compatibilizers on the mechanical and rheological properties of PLA/PBAT blends. RSC Adv 5:73842–73849. https://doi.org/10.1039/C5RA11019J
33. Uneyama T, Doi M (2005) Density functional theory for block copolymer melts and blends. Macromolecules 38(1):196–205. https://doi.org/10.1021/ma049385m
34. Hemelrijck EV, Puyvelde PV, Macosko CW, Moldenaers P (2005) The effect of block copolymer architecture on the coalescence and interfacial elasticity in compatibilized polymer blends. J Rheol 49(3):783–798. https://doi.org/10.1122/1.1888625
35. Srithep Veang-inO, Morris Y, Aussawasathien J, Worajittiphon D P (2023) Stereocomplex PLLA–PBAT copolymer and its composites with multi-walled carbon nanotubes for electrostatic dissipative application. e-Polymers 23(1):1–11. https://doi.org/10.1515/epoly-2023-0089
36. Zhang Y, Zhang W (2025) Effects of block copolymer compatibilizers and interfacial entanglements on strengthening immiscible glassy polymer blends. Macromolecules 58(5):2484–2493. https://doi.org/10.1021/acs.macromol.4c02848
37. Qian J, Dunn CB, Qiang Z (2023) Design of copolymer-based blend compatibilizers for mixed plastic recycling. Macromol Chem Phys 224(24):2300291. https://doi.org/10.1002/macp.202300291
38. Stevels WM, Bernard A, Witte PVD, Dijkstra PJ, Feijen J (1996) Block copolymers of poly($_L$-lactide) and poly(ε-caprolactone) or poly(ethylene glycol) prepared by reactive extrusion. J Appl Polym Sci 62(8):1295–1301. https://doi.org/10.1002/(SICI)1097-4628(19961121)62:8<1295::AID-APP20>3.0.CO;2-5
39. Kim BJ, White JL (2003) Continuous polymerization of lactam–lactone block copolymers in a twin-screw extruder. J Appl Polym Sci 88(6):1429–1437. https://doi.org/10.1002/app.11792
40. Weng S, Xia Z, Chen J, Gong L, Xu R (2012) In situ synthesis of multiblock copolymers of poly(ε-caprolactone) with different poly(ether diols) based polyurethane by reactive extrusion. J Appl Polym Sci 124(5):3765–3773. https://doi.org/10.1002/app.35366
41. Terzopoulou Z, Zamboulis A, Bikiaris DN, Valera MA, Mangas A (2021) Synthesis, properties, and enzymatic hydrolysis of poly(lactic acid)-*co*-poly(propylene adipate) block copolymers prepared by reactive extrusion. Polymers (Basel) 13(23):4121. https://doi.org/10.3390/polym13234121
42. Terzopoulou Z, Zamboulis A, Bikiaris ND, Margellou A, Valera MA, Mangas A, Koltsakidis S, Tsongas K, Tzetzis D, Triantafyllidis K (2024) Properties of PLA-*co*-PBSu copolymers rapidly synthesized by reactive processing. J Polym Environ 32:316–330. https://doi.org/10.1007/s10924-023-02981-0
43. Ding Y, Lua B, Wang P, Wang G, Ji J (2018) PLA-PBAT-PLA tri-block copolymers: effective compatibilizers for promotion of the mechanical and rheological properties of PLA/PBAT blends. Polym Degrad Stab 147:41–48. https://doi.org/10.1016/j.polymdegradstab.2017.11.012
44. Hiemenz PC, Lodge TP (2007) Polymer chemistry. CRC, New York
45. Casas A, Ramos MJ, Rodríguez JF, Pérez Á (2013) Tin compounds as Lewis acid catalysts for esterification and transesterification of acid vegetable oils. Fuel Process Technol 106:321–325. https://doi.org/10.1016/j.fuproc.2012.08.015
46. Sedush NG, Chvalun SN (2015) Kinetics and thermodynamics of $_L$-lactide polymerization studied by differential scanning calorimetry. Eur Polym J 62:198–203. https://doi.org/10.1016/j.eurpolymj.2014.11.038
47. Kricheldorf HR, Weidner SM (2025) H_2O-initiated polymerization of $_L$-lactide. J Polym Environ 33:2843–2857. https://doi.org/10.1007/s10924-025-03565-w
48. Wu D, Lv Y, Guo R, Li J, Habadati A, Lu B, Wang H, Wei Z (2017) Kinetics of $Sn(Oct)_2$-catalyzed ring opening polymerization of ε-caprolactone. Macromol Res 25(11):1070–1075. https://doi.org/10.1007/s13233-017-5148-z
49. Báez JE, Ramírez-Hernándeza A, Marcos-Fernández Á (2010) Synthesis, characterization, and degradation of poly(ethylene-*b*-ε-caprolactone) diblock copolymer. Polym Adv Technol 21(1):55–64. https://doi.org/10.1002/pat.1399
50. Chrysafi I, Ainali NM, Bikiaris DN (2021) Thermal degradation mechanism and decomposition kinetic studies of poly(lactic acid) and its copolymers with poly(hexylene succinate). Polymers 13(9):1365. https://doi.org/10.3390/polym13091365
51. Burgos N, Martino VP, Jiménez A (2013) Characterization and ageing study of poly(lactic acid) films plasticized with oligomeric lactic acid. Polym Degrad Stab 98(2):651–658. https://doi.org/10.1016/j.polymdegradstab.2012.11.009
52. Jang H, Lee J, Kwon MK, Seo KH, Cho KS (2021) Analysis of PLA blends using weighted relaxation spectrum. Fibers Polym 22(2):314–322. https://doi.org/10.1007/s12221-021-0121-z
53. Tábi T, Hajba S, Kovács JG (2016) Effect of crystalline forms (α′ and α) of poly(lactic acid) on its mechanical, thermo-mechanical, heat deflection temperature and creep properties. Eur Polym J 82:232–243. https://doi.org/10.1016/j.eurpolymj.2016.07.024